Journal of Sciences, Islamic Republic of Iran 29(4): 341 - 359 (2018) http://jsciences.ut.ac.ir
University of Tehran, ISSN 1016-1104

Petrology, Geochemistry and Tectonomagmatic Evolution of Hezar Igneous Complex (Rayen- South of Kerman- Iran): the First Description of an Arc Remnant of the Neotethyan Subduction Zone

M. Noorizadeh[1*], A. Moradian[1], H. Ahmadipour[1], M. R. Ghassemi[2], J. F. Santos[3]

[1] *Department of Geology, Faculty of Science, Shahid Bahonar University of Kerman, Kerman, Islamic Republic of Iran*
[2] *Research Institute for Earth Sciences, Geological Survey of Iran, Meraj Ave., Azadi Sq., Tehran, Islamic Republic of Iran*
[3] *Department of Geosciences, Geobiotec Research Unit, University of Aveiro, 3810-193 Aveiro, Portugal*

Received: 28 July 2016 / Revised: 3 June 2017 / Accepted: 19 July 2017

Abstract

The Hezar Igneous Complex (HIC) in the south-eastern part of Urumieh-Dokhtar magmatic arc, is the most prominent magmatic feature in the Kerman Porphyry Copper Belt, that understanding magmatic evolution of which may shed light on the tectonomagmatic development of this less-studied part of an important magmatic arc in the Neotethys realm. The HIC has been developed in the the intersection of the NS-striking Sabzevaran fault and the NW-SE striking Rafsanjan-Rayen fault. It is indicated that the possible place of the conduit and vent is in Jalas Mountain which has been splitted later by the Sabzevaran fault into Minor and Major Jalas. The current summit had been constructed by ascending magma chamber under the HIC that constitutes the Kamali Mountain at the south of the summit. Some plutonic rocks of the HIC are exposed at Kamali Mountain. The subalkaline rocks of this complex mainly are composed of different pyroclastic and lava flow rocks, acidic to basic in composition, showing the evidences of fractional crystallization and mineral segregation. Sequential explosive and effusive eruptions with Strombolian to Vulcanian types are evident in the successive volcanic layers. The compositional trend shows the melting of spinel lherzolite, not garnet lherzolite. The subduction-related mechanism of the magma genesis has been indicated by IAB nature of the magma formation in geochemical diagrams.

Keywords: Hezar Igneous Complex (HIC); Rayen; Urumieh-Dokhtar magmatic arc; Tectonomagmatic evolution; Whole-rock geochemistry.

[*] Corresponding author: Tel: +989155516016; Fax: +985162424781; Email: nooorizad@gmail.com; noorizadeh@tvu.ac.ir

Introduction

The Urumiyeh-Dokhtar magmatic arc (UDMA) – the Iranian segment of the volcanic arc of Alpine-Himalayan or Neotethyan convergent belt- is parallel to Zagros orogenic belt with its NW-SE strike and is one of the major manifestations of convergence between the Eurasia and Gondwana. The Dehaj-Sarduieh volcano-plutonic belt – as part of the Urumiyeh-Dokhtar magmatic arc- and especially its Kerman Cenozoic magmatic arc (KCMA) plays a significant role in the formation of copper deposits, which are related to Miocene intrusive bodies, which have been intruded and emplaced in Eocene sedimentary-volcanic successions [1]. Despite extensive new studies in Neotethyan realm, the Iranian part of this convergent zone –especially its south-eastern part- is remained less studied and less documented than the other parts – i.e. Himalayas, Alps or Anatolia [2]. This arc is a result of closure of Neotethys and the subduction of oceanic crust under Central Iran in island arc, continental arc, and collision setting. It was indicated through geochemical and geochronological studies that UDMA was an active continental margin during subduction of Neotethys oceanic lithosphere under Central Iran microcontinent [3].

The relation between the faults and seismicity has been studied in different papers. According to these studies and by using geomorphological observations in Kerman province, it has been shown that the north-south dextral strike-slip fault (Sabzevaran in the south-east of Iran which extended to Hurmoz strait between Oman Sea and Persian Gulf) is linked to other inner right-lateral faults of Central Iran (such as Lalehzar fault as a part of Rayen- Rafsanjan fault system, passing through Shirinak village where is located in the southern flank of Hezar, cutting the southern part of Hezar including its vent(s)and crater(s) and making possible that a great alteration taking place in this part) which makes a place facilitating the extrusion and intrusion of Hezar Igneous Complex (HIC). Integration of strike-slip and dip-slip components along active margins of tectonic plates leads to formation and development of strike-slip duplex faults in this magmatic arc which makes a fault control for copper mineralization in Porphyry Copper Deposits (PCDs)[4]. It seems that the same process has led to the formation of HIC. The relationship of these PCDs with Hezar complex is implied in some works. There are three major clusters of PCDs in KCB: Miduk, Sahrcheshmeh, and Daraloo, all of which are intrusive boddies in this complex or their conterparts [5]. Different studies suggest that the processes such as slab breakoff [6] and remobilizaed subduction leads to fertility of these Mid Miocene magmas making most of the largest porphyry Cu-Mo deposits (as Sarcheshmeh and Miduk) [7]. In north-western part of UDMA, calc-alkaline magmatism in early Oligocene gives way to shoshonitic plutonism in late Oligocene. Geochronological and geochemical evolution of arc magmatism from early preceding volcanic into more evolved magmas, indicates the maturation of arc magmatism [8], [9]. Diachronous character of collision in UDMA was due to irregular shape of Arabian indents [10], [11].

Arc-related properties of the southern intrusive neighbor –i.e. Bahr Aseman complex- have been indicated in some recent works. In southern part of HIC, in Bahraseman complex, copper deposits of Takht Gonbad with shallow granodiorite porphyries are intruded in pyroclastic rocks in late Oligocene. A change in subduction mechanism in late Cretaceous, modified the dip angle of subducted slab and moved the subduction front from Sanandaj-Sirjan, landward and made the Bahr Aseman complex. This shallowing leads to an extensive volcanism including Razak and Hezar complexes in Eocene and Oligocene respectively [12], [13].

A granitoid body – i.e. Lalehzar Mountain- which is located to the west of the HIC has been studied in a recent study and as the other magmatic trends of UDMA the continental arc origin of this I-type granitoid is verified [14].

Few studies [15], [16] and a detail geological report by mapping team of Rayen 1:100k geological map [17] are all the resources dealing with HIC in detail. Dimitrijevic (1973), has demonstrated the stratigraphic relations between Hezar volcano-sedimentary products and other materials surrounding them. Maleki (2004) has drawn a stratigraphic sequence of the pyroclastic and lava sequences of a limited part of northern flank of Hezar. But its geochemical data especially trace elements' data shows very big errors. Kajejavaran (2010), on the other hand, take advantage of more accurate geochemical data of a limited section of Hezar. Only some limited parts of the northern flank of the HIC have been investigated through the above studies. Then, despite invaluable data provided, a comprehensive image of the Hezar evolution has not been explained through these works. Furthermore, all of the previous resources have mentioned basaltic to andesitic materials extruded from Hezar and their pyroclastic counterparts. Finding other more acidic volcanic rocks was one of our goals in the field studies. Besides, uplift and vast erosion is a case because of active tectonics of the region. Then it would be expected that some intrusive rocks were exposed on the surface, which were not

reported in previous works- even in geological maps provided.

Geological Setting and socio-economic significance of HIC

The Rayen tourist town is among the ancient regions of Kerman province which is located in 100 km SE of Kerman and 1079 km SE of Tehran. The studied area is located at the west of Rayen, between 29°25′00″N, 57 10′00″E and 29°35′00″N, 57 25′00″E.

Almost all of tourist attractions of Rayen are directly or indirectly related to Hezar Mountain which is a part of Hezaran mountainous area (that is, Hezar and Bidkhun). Some of these geotourism attractions are as follow [18], [19]: the highest summit of the province and the fourth in Iran (4501m); the third highest cities of Iran (Baft); the highest residential villages in Iran (Babzangi and Ordikan with 3300 m elevation above the sea level); the minimum gravity of Iran (distance from the earth's center is 1200m more than that of Damavand- the highest summit of Iran (5650m)) [20]; the high extent and diversity of plant species which are used as medicinal plants, which is the main reason of nomenclature of Hezar. "Hezar" that means "thousand" in Farsi, is used for this mountain because of this local suppose that there are more than one thousand medicinal plants all around this mountain. So collecting and processing medicinal plants is usual among inhabitants. Some plant species are discovered in Hezar for the first time, such as *Ferula hezarlalehzarica* which takes its name from this mountain; (6) widespread metal mine districts and potentials around the mountain (such

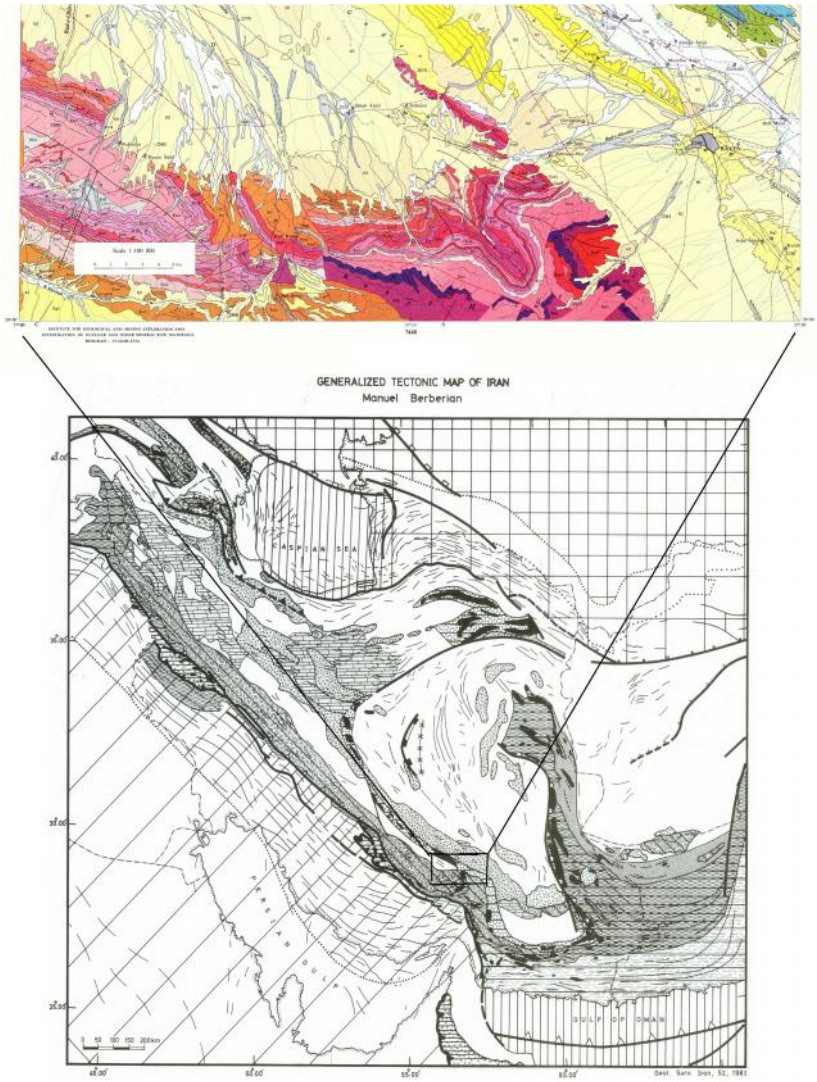

Figure 1. The approximate location of the study area on tectonic map of Iran [2] and 1/100.000 geological map of Rayen.

as Dor-Alou at south) which is evident in industrial and artistic handicrafts of this region ; valuable ornamental and facade structural stones' historical mines such as travertine and green marble, around the mountain (some used in construction of Taj-Mahal, India); and its drainage system and rivers (such as Tahroud and Jiroft) flowing on the flanks of Hezar, water down major parts of this arid region and making a very diverse climatic conditions.

Despite the significance of the evolution of Hezar in understanding the events of this region, there are no comprehensive work dealing with it, because of the following reasons: (1) the highly intricate structures due to active tectonics; (2) the vast area of the Hezar Igneous complex (HIC) (900 km^2); (3) high elevation (4501m) and prominence (2741m); (4) difficult access in southern, eastern and western flanks of Hezar; (5) climatic limitations due to variable weather conditions and snow-covered lands; and (6) previous lack of security because of transit of drugs by drug traffickers and gangs which is not of concern now [21]. (7) lying on the borders of two 1/100k geological maps (Rayen and Sarduieh) with different teams, different color systems and different field interpretations.

Materials and Methods

312 rock samples were collected from which 190 were selected for detailed petrographical studies. Then, 40 samples were selected for geochemical analysis taking into account the diversity of rock units and the location of the outcrops. These analyses were done at SGS Co. (Australia and Canada branches) using borate fusion XRF (code: GC XRF76V) for major elements and sodium peroxide fusion combined ICP-AES and ICP-MS (code: GE ICM90A) for trace elements. Topographic maps were drawn using mainly Google Earth™, TCX convertor, and Quik Grid. For geochemical plots and calculations, GCDkit version 4.00 software and its R console with Microsoft Office Excel was used.

Results

Field and geomorphological Investigations

Most of studies on this area are restricted to the north-eastern part of this igneous complex mainly due to lack of appropriate accessibility and asphalt roads (other causes are previously mentioned). The study gap on the southern flank – which involves most of field clues solving the problems of the evolution of Hezar - has led

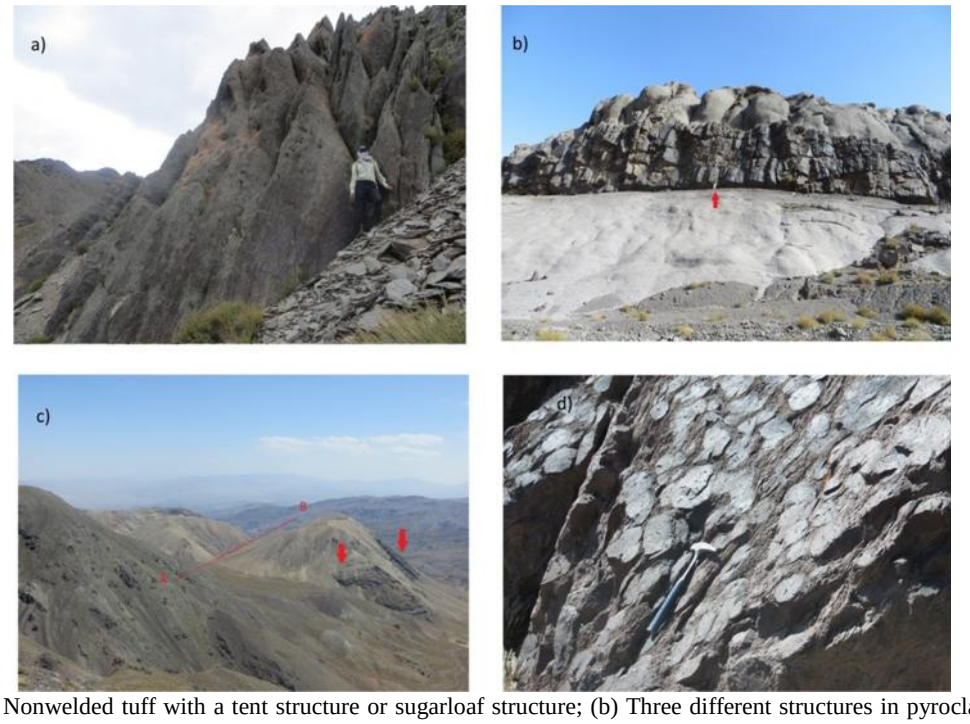

Figure 2. (a) Nonwelded tuff with a tent structure or sugarloaf structure; (b) Three different structures in pyroclastic rocks; a layer of welded tuff is located between two volcanic surge deposits. The arrow shows the place of a person as a scale. (c) Jalas mountain is a plug or volcanic dome of acidic composition which is cut by a piece of north- south fault system (a-b respectively) into Minor and Major Jalas. The arrows show the place of the relict layers of Hezar volcanic successions raised by extrusion of Jalas. It might be the main place for the conduit of the HIC. (d) Summit agglomerate is a conclusive evidence that the current summit had not been the place of the vent or conduit of Hezar.

to the lack of a comprehensive understanding about the formation of this complex.

According to the field evidences, HIC, is not merely a single volcanic edifice. It is a part of a huge stratovolcano which its southern part had been eliminated due to a caldera collapse or by the elongated Rafsanjan- Rayen fault zone. Then, main part of the southern flank, including conduit(s) and vent(s) is crushed and eroded with different transportation agents.

There are some field evidences supporting the above idea: a) The southern fault valley (Ziarat-Chartagh) is a part of Rafsanjan- Rayen fault system. b) Alteration have been facilitated by the appropriate conditions made by these fault ruptures (or caldera) and the subsequent penetration of hydrothermal solutions derived from magma chamber in later phase of magmatism. c) HIC volcanic successions can be correlated with volcanic layers of the southern valley (Ziarat-Chartagh) on the northern flanks of Bahraseman intrusive body. d) Besides, these fractures – which is extended from Shirinak village to the southern part of the Hezar mountain- have made an appropriate place intruding coarse-grained intrusions under the Hezar summit (4501m) -outcropped in Kamali mountain- and uplifting the HIC as the highest mountains of the province which lead us to this implication that the ascent of magma chamber may be the main reason for uplift of Hezar and its disintegration especially in southern part; and e) Sills, dykes and subvolcanic intrusions are mainly evident in southern side of southern valley which are the last volcanic phases.

The major fault trends in the region are the result of the intersection of two major dextral (right-slip) fault systems (i.e. NE-SW Sabzevaran fault which reaches to the Hormuz strait in the boundary of Persian Gulf and Oman Sea, and NW-SE Rayen-Rafsanjan fault) which has made a suitable environment for extrusion of igneous materials. Although, uninterrupted and continuous activity of these faults has made the southern part of Hezar disintegrated including the conduit(s) and vent(s). The features caused by the intersection of these faults are evident everywhere on this region. One of which is obvious in Jalas Mountain – one of the southern HIC intrusions on north-west of Ziarat village- which is divided to two distinct sections – the Lesser Jalas and the Greater Jalas (Figure 2c). Apparently, Jalas which had been intruded by the action of the intersecting faults, segmented into two parts subsequently with continued displacements of these faults. Uplifting Jalas Mountain on which some evidences of relict uplifted volcanic successions of Hezar are remained, might be the location of Hezar main conduit.

The movement path of the last phase of glacial bodies, before the recent climate change and multiple draughts in Kerman province, is indicated by abundance of glacial erratics merely on north-eastern flank which is disappeared to the north with a very sharp boundary. However, these erratics have lain on fine-grained subglacial moraine making an appropriate place as groundwater reservoir and suitable agricultural land for Rayen district. Rayen residents have used this potential by using qanats (karizes) and goorabs (i.e. small scale earth dams lead some part water current into the earth supplying the groundwater) that could be obviously seen in the satellite images.

The Hezar Mountain is surrounded by an incomplete ring of volcano-sedimentary layers in north-eastern and eastern parts which makes a feature like an asymmetrical trap-door caldera.

Linear alteration evidence is obviously seen in the southern flank on satellite images. Although, it is visible as point structures on eastern and northern flanks, some of which have been exploited as globally famous green marble and travertine of Rayen from long time ago.

There are four different lithological units in the study area:

1): Pyroclastic and volcano-sedimentary layers making the main part of the HIC. This unit includes welded and non-welded tuffs, and some agglomerates, pyroclastic surges and volcanic breccia making different strata showing different phases of volcanism with sharp boundaries (Figure 2b). Some of the tuffs show structures such as accretionary lapilli. Non-welded tuffs show erosional structures such as tent-like erosion of sugarloaf structures (Figure 2a). Some evidences of flow structures can be seen in volcanic surges in which some fragments and clasts of the previous rocks are remained and verify the currents. Occurrence of agglomerate in summit (4501m) may indicate that the current summit was not the summit or the vent at the time of extrusion (Figure 2d). Because this agglomerate indicates that this place was at a lower height and was made due to a current flowing to this place. The later uplift of the summit may be the result of rising of the magma chamber which is evident in Kamali.

2): Lava flows which are interbedded with pyroclastic layers are not as widespread as them. These layers sometimes show columnar or prismatic structures in some parts of southern flank of HIC around Ziarat village.

3): Subvolcanic bodies which make dikes, sills and some rhyolite domes. These structures are gechronologically significant because of their main role in dating the last phase of magmatism in this region. Among these units Jalases (minor and major) are the

most massive bodies. Minor Jalas and Major Jalas were both one massive plug or volcanic dome which have cut by a north-south trending fault. Field investigations indicates that Jalas was probably the place of volcanic vent (or one of the vents) of HIC.

4): Some plutonic bodies which have been raised along the southern fault. One of the most significant such bodies, Kamali, on the southern flank of the summit is composed of gabbro and diorite.

Petrography

As mentioned before four distinct rock units are found in HIC. The north-eastern part of the HIC, is mainly composed of andesitic and basaltic rocks within huge volumes of pyroclastic rocks. The pyroclastic rocks can be divided into pyroclastic falls and flows (Figure 3b), as volcanic tuffs, agglomerates, breccias, and surge deposits.

In particular, sub-volcanic bodies such as dikes, sills

Figure 3. Some microphotographs of different rock types in HIC: a) A decomposing amphibole crystal in an andesitic basalt; b) Flow texture in a pyroclastic rock whose pores filled with secondary products such as calcite; c) Rhyolite with columnar structure in Minor Jalas under the microscope; d) a diorite with granophyric texture (quartz and K feldspar) from Kamali intrusion; e) Gabbro with a subhedral opaque mineral. The section is slightly thicker than usual. Pyroxene is replaced with secondary minerals such as chlorite, epidote and Fe oxides. f) Consertal intergrowth texture in Gabbro, showing some plagioclase crystals growing among the K feldspars. g) Basalt full of two generations of plagioclase crystals with clinopyroxenes; h) Another basaltic sample showing overgrowth and sieve textures in plagioclase phenocrysts.

and plugs, sometimes with columnar habit must be mentioned (Figure 3c). The main factor for their relevance in interpreting HIC evolution is that they testify for the latest phase of magmatism in HIC, because they are evidently younger than the successions and masses that they had intruded. These sub-volcanic bodies possess a variety of chemical compositions: from basic rocks with two or more generations of plagioclase some of which show a sieve textures with signatures of solution and recrystallization and decomposed pyroxenes, through intermediate rocks with microlithic texture showing a flow direction (trachytic texture), to acidic rocks with granular texture of quartz and plagioclase and some sphene as an accessory phase.

The other first-time studied rock unit in the region is gabbroic – dioritic intrusive masses that their emergence may cause distinct height of the summit (4501m) and the altitude of southern flank, that are evident in Jalas intrusion (minor and major) and Kamali intrusion (**Figure** 3d,e, and f). These intrusive masses are of mafic and intermediate rocks (gabbro and diorite) which are mostly composed of calcic plagioclases and pyroxene (both clinopyroxene and orthopyroxene, sometimes twinned accompanied by minor long crystals of apatite and euhedral iron oxide) , but there are some limited parts of felsic rocks outcropped in some parts of Kamali intrusion just below the summit which are distinct from previous bodies with a greater amount of K- feldspars and quartz crystals and less amount of plagioclase.

Certainly, most of mafic minerals are altered through late processes into other products (such as brucite, chlorite, epidote, iron oxide, etc.).

The multiple processes of solution and recrystallization are evident in feldspar crystals with sieve texture and their clear margins without any dusty view. Moreover, there are some evidence of twinning, glomerocrystic texture and two or more evolutionary generations in the feldspars of some samples (Figure 3g and h).

Acid rocks which are the final extracts of magma differentiation are very rare and these rare products predominantly have undergone alteration, so that the fresh acid samples are not widespread around the region. In rhyolite porphyry samples, it can be seen that calcite and chlorite replaced the mafic minerals. Feldspar minerals (mainly plagioclase) are altered and sometimes show sieve texture. Biotite, which is very rare, is decomposed in margins and some kinds of iron oxide are released (Figure 3a).

Trachitic texture is evident in some basalts and andesites which is made by flow orientation of microlithic laths of plagioclase minerals. However, there are some aggregations of larger feldspar crystals (glomerocrysts).

Abundance of calcite among pyroclastic deposits may be attributed to falling out of these materials in a shallow lake. Besides, there is some evidence of other secondary minerals as jasper and epidote which are the products of hydrothermal Ca-bearing hot fluids of late stages of the volcanism that can be seen mainly in southern flank of Hezar. Occurrence of silica and epidote veins may indicate intrusion of plutonic bodies from the lower parts that as mentioned previously is verified by Kamali plutonic rocks (gabbro diorite).

Disequilibrium and overgrowth textures, such as sieve texture in feldspar, show that the crystal has became unstable and have been dissolved due to changes in thermodynamic conditions (especially pressure changes and mixing with a different magma).

Geochemistry

Chemical classification of the rocks of the HIC

The whole rock chemical compositions of Hezar rock units are shown in Table 1. Hezar Igneous Complex includes a wide variety of igneous rocks (basic, intermediate, and acid). As shown in Figure 4, the studied rock samples mainly fall in subalkaline domain (mainly calc-alkaline).

Rock samples studied consist of the following types: 1): Volcanics: which could be classified as: a): Pyroclastics: which constitute the main part of the HIC. These rocks cover a wide variety of the fall and flow materials such as tuff, volcanic breccia and agglomerate, volcano-sedimentary surge deposits; and b): Lava materials: which could be observed as sporadic volcanic layers between voluminous pyroclastic rocks and show a wide spectrum from basic to intermediate and even acid materials. 2): Plutonics: which were encountered in field investigation for the first time in this area and are restricted to Kamali area (south-west of the summit). 3): Subvolcanics: very rare materials which are spread over the limited parts as dikes, sills and small intrusives. This variety is symbolized and shown in the legend in Figure 4. The major element composition of the studied rock samples are as follow: SiO_2 45-70 %wt; TiO_2 0.1-1.7%wt; Al_2O_3 22-37%wt; Fe_2O_3t 1-12%wt; MgO 0.5-5.5% wt; CaO 2-11%wt; Na_2O 1.5-5% wt; K_2O 0.5-5.5 %wt; P_2O_5 0.1-0.7 %wt. But these compositional limits has shown some differences between mafic and felsic (silicic) rocks. The mafic rocks show the following properties: $TiO_2 > 1$%wt; $Fe_2O_3t > 8$%wt; MgO> 3% wt; CaO> 8%wt; $Na_2O < 3$% wt; $K_2O < 2.5$ %wt. Although these ranges in felsic (silicic) rocks are as follow: $TiO_2 < 0.5$%wt; $Fe_2O_3t < 4$%wt; MgO< 1.5% wt; $1.5 < CaO < 8$%wt; $Na_2O > 3$% wt; $6 > K_2O > 1.7$ %wt.

Table 1. Geochemical analysis of 28 rock samples using ICP-MS and XRF with calculated CIPW normative minerals.

ANALYTE	METHOD	S38	S39	S40	S41	S42	S43	S44	S45	S46	S47	S48	S49	S50	S51	S52	S53	S54	S55	S56	S57	S58	S59	S60	S61	S62	S63	S64	S65
Ag	ICM90A	0	0	0	0	0	0	0	0	0	0	2	0	0	0	4	2	2	0	0	0	3	0	0	0	0	0	2	0
As	ICM90A	0	0	22	0	0	0	0	0	0	0	11	0	7	0	0	0	0	6	0	9	15	0	0	0	0	11	0	12
Ba	ICM90A	526	355	509	335	463	533	474	364	277	401	282	365	407	621	398	183	403	446	704	310	567	923	467	311	746	415	357	389
Bi	ICM90A	0.3	0.1	0	0.2	0	0	0	0	0	0	0.1	0	0	0.8	0	0	0.2	0.1	0.2	0	0	0.4	0	0	0	0.1	0	0
Cd	ICM90A	2.9	2.3	2.5	2.3	3.6	0.4	1.1	0.9	0	0.2	1.2	1.9	1	2	1.1	1.8	1.8	2.5	1.4	2.3	1.5	1.8	0.9	2.5	1	2.2	0.6	0.8
Ce	ICM90A	53.3	64.1	83.1	48.9	52.4	41	74.8	39.2	29.9	41.7	39.5	54.8	31.5	34	60.5	35	42.1	46.7	101	53.8	24.1	73.5	50.3	42.6	40.4	81.1	40	56.9
Co	ICM90A	18.1	37.9	24.9	10.1	3.6	26.4	37.9	32.9	41.7	40.6	33.7	5.2	33.6	26.2	26.1	32	9.5	27.7	3.2	28.2	34.5	10.4	5	5.9	28.7	28.7	29.8	31.9
Cr	ICM90A	13	13	18	21	52	23	91	16	92	50	24	19	53	52	31	44	15	36	38	12	22	24	44	10	47	11	60	49
Cs	ICM90A	0.7	2.1	1.6	1.6	1.7	0.7	1.1	0.6	1.1	4.3	7	2	1	0.7	1.6	2.6	0.8	1.2	1	8.2	1.7	2.3	1.9	0.7	1.3	2	1.7	1.3
Cu	ICM90A	86	240	79	38	31	79	568	45	113	95	61	23	109	51	174	104	33	124	24	66	92	33	32	38	64	231	58	72
Dy	ICM90A	1.81	9.86	11.5	4.42	2.4	4.65	5.94	6.11	4.91	5.06	4.7	6.06	5.43	3.85	8.71	4.69	5	5.78	8.19	5.64	4.56	6.07	2.45	4.29	6.38	9.86	6.17	8.08
Er	ICM90A	0.87	6.19	7.22	2.78	1.65	2.93	3.51	3.89	3.13	3.08	3	3.9	3.49	2.44	5.34	2.94	3.2	3.56	5.91	3.62	2.9	3.95	1.74	2.89	4.05	5.99	3.84	5.18
Eu	ICM90A	1.35	2.55	3.04	1.46	1	1.66	2.37	1.95	1.59	1.81	1.44	1.62	1.49	1.18	2.18	1.56	1.75	2.3	0.97	1.8	1.58	1.49	1.04	1.59	1.88	2.33	1.7	2.06
Ga	ICM90A	20	18	16	18	12	15	13	20	15	16	15	15	16	12	18	15	17	18	14	16	15	21	12	15	15	21	16	17
Gd	ICM90A	3.34	10.1	11.9	5.24	2.78	4.92	7.03	6.15	4.79	5.34	4.91	5.89	5.27	3.66	8.78	4.91	5.19	6.15	8.29	6.03	4.46	6.97	2.9	4.5	6.28	11.2	6.22	8.2
Ge	ICM90A	0	1	1	1	1	1	1	1	1	1	1	0	1	0	0	1	0	1	0	0	0	1	1	0	0	2	0	0
Hf	ICM90A	4	6	8	5	6	4	5	4	3	3	4	7	3	5	6	3	4	4	10	5	3	8	5	5	5	8	5	6
Ho	ICM90A	0.27	1.89	2.14	0.92	0.45	0.88	1.07	1.15	0.89	0.91	0.89	1.12	1.03	0.71	1.63	0.87	0.95	1.06	1.58	1.07	0.89	1.27	0.47	0.81	1.2	2.07	1.15	1.51
La	ICM90A	29	24.6	34.4	20.1	25.3	17.1	32.6	14.5	11.5	19.1	16.5	24.8	15	22.6	26.1	15.1	19.4	21.1	52.9	25.4	9	41.8	26.7	19.7	17	36.5	16.7	24.5
Li	ICM90A	125.1	55.1	45.1	40.1	22.1	74.1	71.1	70.1	29.1	50.1	69.1	14	28	0	18	10	11	0	0	12	32	11	25	16	29	40	31	15
Lu	ICM90A	0.1	0.79	0.94	0.49	0.32	0.43	0.47	0.52	0.44	0.39	0.41	0.58	0.47	0.41	0.73	0.42	0.49	0.48	0.91	0.52	0.39	0.69	0.35	0.45	0.58	0.93	0.56	0.72
Mo	ICM90A	0	0	3	0	0	0	0	0	0	0	0	0	0	0	4	0	0	4	0	3	0	0	0	0	0	5	0	0
Nb	ICM90A	5	11	11	6	8	4	16	7	4	4	8	14	5	6	9	4	5	8	24	10	2	22	8	5	6	16	7	10
Nd	ICM90A	22.6	35.5	45.1	22.8	17.9	19.5	35	21.6	16.5	21	19.2	23.8	18	14.8	32.9	17.9	21.1	23.1	39.2	24	14	30.8	17.9	20.7	22.2	43.2	22	30.4
Ni	ICM90A	14	8	0	0	0	8	36	0	32	42	16	0	34	5	9	24	0	7	0	9	10	5	0	0	17	0	19	12
Pb	ICM90A	51	21	31	11	28	16	25	31	19	15	28	17	29	26	13	15	28	18	23	20	12	19	30	21	23	54	19	24
Pr	ICM90A	5.94	8.13	10.4	5.61	5.16	4.76	8.74	4.98	3.76	4.91	4.65	6.09	4.01	3.78	7.52	4.29	4.98	5.52	10.7	6.09	3.11	8.15	5.1	5.07	5.08	9.98	5	7.13
Rb	ICM90A	53.9	42	67.4	64.7	93.5	36.4	27.7	23.1	24.7	27.8	132	94.9	17.3	64.7	60.5	33.7	53.5	59.1	165	114	42.5	197	95.6	46	43.2	23.2	19.4	51.2
Sb	ICM90A	0.7	1.5	1	0	0	0	0	0	0	0	0.7	0	0	0	0.6	0	0	4.9	0	0	0	1.3	0	0.8	0	1.1	0	0

Sc	ICM90A	7	7	7	8	8	7	6	7	7	7	6	8	6	8	7	7	6	6	7	6	6	8	7	7	6	8	7	6
Sm	ICM90A	3.8	8.8	10.5	4.9	3	4.3	6.8	5.4	4.2	4.8	4.3	5.2	4.4	3.4	7.8	4.3	4.7	5.4	7.7	5.5	4	6.5	3	4.3	5.8	10.3	5.2	7.4
Sn	ICM90A	1	3	2	1	1	2	1	1	1	1	2	3	2	2	4	2	2	5	4	2	0	3	2	2	2	4	2	2
Sr	ICM90A	732	466	688	506	267	527	686	587	607	690	314	284	472	604	535	477	619	683	574	581	507	654	280	456	1057	643	580	617
Ta	ICM90A	1.2	1.1	1	0.7	0.8	0	1.4	0.7	0	0	0.8	1.3	0	0.6	0.8	0	0	0.7	2.4	0.9	0	1.9	0.8	0	0.6	1.2	0.6	0.9
Tb	ICM90A	0.35	1.56	1.81	0.77	0.39	0.72	1	0.94	0.77	0.81	0.74	0.91	0.83	0.57	1.36	0.76	0.78	0.89	1.23	0.9	0.74	1.03	0.38	0.67	0.98	1.67	0.96	1.28
Th	ICM90A	9.6	7.9	10.6	7.4	11.6	6.7	2.9	4.6	3.6	6.9	5.4	10.9	3.9	8.6	7.9	4.3	4.6	7.7	44.2	12.6	2.5	22	11.2	5.7	4.3	12.5	4.4	8.4
Tl	ICM90A	0	0	0	0	0	0	0	0	0	0	0.5	0	0	0	0	0	0	0	0.6	0	0	0.7	0	0	0	0	0	0
U	ICM90A	2.57	1.94	2.62	1.66	2.47	1.42	0.77	1.19	0.89	1.48	1.26	2.24	0.98	2.14	1.92	0.92	1.1	1.82	9.94	2.76	0.51	5.44	2.41	1.31	1.3	3.01	1.32	2.17
V	ICM90A	120	270	60	50	10	220	200	240	300	310	230	30	280	260	250	270	30	200	20	190	280	40	10	30	270	230	260	250
W	ICM90A	2	3	3	2	2	2	2	2	2	2	2	2	1	2	4	1	4	2	2	3	1	3	2	2	2	3	3	2
Y	ICM90A	7.5	50.1	47.9	23.7	12.3	21.6	23	31.1	21.9	21.4	24.5	32	26.2	20.4	41.7	21.1	25.5	28.1	43.8	27.3	20.6	40.4	12.6	20.1	28.6	54.8	28.1	36.1
Yb	ICM90A	0.6	4.8	5.6	3	1.8	2.6	2.8	3.1	2.5	2.4	2.4	3.4	2.8	2.3	4.3	2.4	2.9	2.8	5.4	3.1	2.4	4.3	1.8	2.6	3.3	5.8	3.2	4.2
Zn	ICM90A	100	110	130	60	50	80	90	100	100	100	120	70	90	110	110	70	100	90	10	100	80	40	50	80	100	110	90	110
OI	XRF76V	3.59	2.98	2.78	2.43	1.15	3.3	2.17	1.83	2.69	2.66	10.5	2.99	2.61	1.52	2.33	1.16	3.07	1.42	1.02	0.83	4.16	2	0.73	2.49	5.57	5.51	3.55	1.82
SiO2	XRF76V	60.5	50	55.4	60.8	71.3	54.2	51.3	49.9	49.2	47.5	46.1	67.1	49.6	68.9	51.4	50.3	58	50.9	69.2	53.7	47.7	61.7	70	60.4	49.3	52.1	51.1	51
Al	XRF76V	17.2	16.4	16.1	16.5	15.2	17.8	17.1	19.7	17	18.3	16.3	15.4	18.5	14	18.9	18.7	18.2	17.7	14.4	18.1	18	17.1	15	16.7	17.1	14.6	17.2	18.1
Fe2O3	XRF76V	4.61	12.9	10.8	4.95	1.96	8.69	10.1	10.5	11	10.9	9.38	4.23	11.1	3.96	10.5	10.1	7.48	10.9	1.89	9.93	11.5	4.75	2.09	5.13	10	11.1	10.2	10.9
MgO	XRF76V	2.2	3.09	2.18	1.56	0.45	3.59	5.11	3.11	5.52	5.39	3.58	0.92	4.97	1.2	2.79	5.27	1.55	3.22	0.55	3.29	4.73	0.99	0.45	1.28	3.08	2.82	3.87	3.42
CaO	XRF76V	4.44	8.33	5.3	4.32	1.92	5.04	8.43	9.1	9.89	9.57	8.47	2.13	9.15	2.2	8.95	9.2	6.03	8.06	2.37	8.15	8.81	3.62	2.01	4.33	6.66	7.32	8.74	8.5
K2O	XRF76V	2.29	1.75	2.89	2.01	2.9	1.62	1.78	1.13	1.07	1.34	2.93	2.29	1.03	2.91	2.22	1.28	2.17	1.88	5.02	2.26	1.45	5.36	2.8	1.79	1.95	0.98	1.13	2.06
Na2O	XRF76V	4.78	2.17	3.31	4.32	4.76	4.98	2.62	3.12	2.81	2.52	1.72	4.83	2.5	4.1	2.32	3.01	3.4	3.85	3.81	3.49	2.2	3.98	4.79	4.7	4.61	3.06	2.53	2.78
TiO2	XRF76V	0.71	1.67	1.36	0.41	0.21	0.87	1.27	1.18	1.1	1.18	0.99	0.47	1.25	0.36	1.33	1.04	0.51	1.21	0.33	1.07	1.11	0.6	0.21	0.38	1.21	1.62	1.17	1.45
MnO	XRF76V	0.07	0.21	0.21	0.14	0.09	0.18	0.16	0.15	0.18	0.19	0.2	0.09	0.18	0.07	0.15	0.17	0.17	0.21	0.02	0.18	0.19	0.06	0.14	0.17	0.16	0.2	0.17	0.18
P2O5	XRF76V	0.28	0.47	0.65	0.22	0.08	0.22	0.67	0.29	0.21	0.24	0.24	0.1	0.25	0.1	0.44	0.23	0.26	0.37	0.09	0.3	0.17	0.19	0.07	0.26	0.29	0.58	0.3	0.35
Cr2O3	XRF76V	0	0	0	0	0	0	0.02	0	0.01	0	0	0.48	0	0	0	0	0	0	0	0	0	0	0	0	0	0	0	0
V2O5	XRF76V	0.02	0.04	0.02	0	0	0.04	0.04	0.04	0.04	0.06	0.04	0	0.05	0.01	0.05	0.05	0	0.03	0	0.03	0.05	0	0	0	0.04	0.04	0.05	0.05

The Mg number (Mg#=Mg/Mg+Fe) in felsic rocks (25-40) is evidently lower than that of mafic rocks (30-58). This may suggest that the felsic magma is more evolved (far from the mantle composition). This may be verified by low Cr content (<100 ppm) and low Ni content (<50 ppm) [22]. But this feature is evident in all samples (mafic and felsic).

In major element diagrams proposed by Irvine and Baragar (1971) and Miyashiro (1974) (not shown here), some samples (especially basic ones) show tholeiitic affinity, however this affinity has not been verified by trace element diagrams [23], [24]. It may be due to anhydrous fractionation which shifts the sample plots to higher FeO contents versus MgO, but it has no effect on the trace element signatures of the above diagrams. It may be the result of the mobility of the major elements due to a low-grade metamorphism. The differences between the domains of various diagrams of total-alkali versus silica by different authors can be interpreted by the same implication (Figure 4).

Some of the emplacement processes for igneous rocks may be inferred by Harker diagrams of compatible and incompatible elements versus SiO_2 (not shown here but like Figure 5). It seems that during the differentiation of ferro-magnesian minerals such as olivine and clinopyroxene, the concentration of compatible elements (Co, Cr and Ni) decreases, however, the concentration of incompatible elements (Th, La and Ba) increases. This effect is accompanied by a breaking point in SiO_2=55% or MgO=3%wt in most of these Harker diagrams. Eliminating the samples 19 and 22 makes the trends more obvious. Low contents

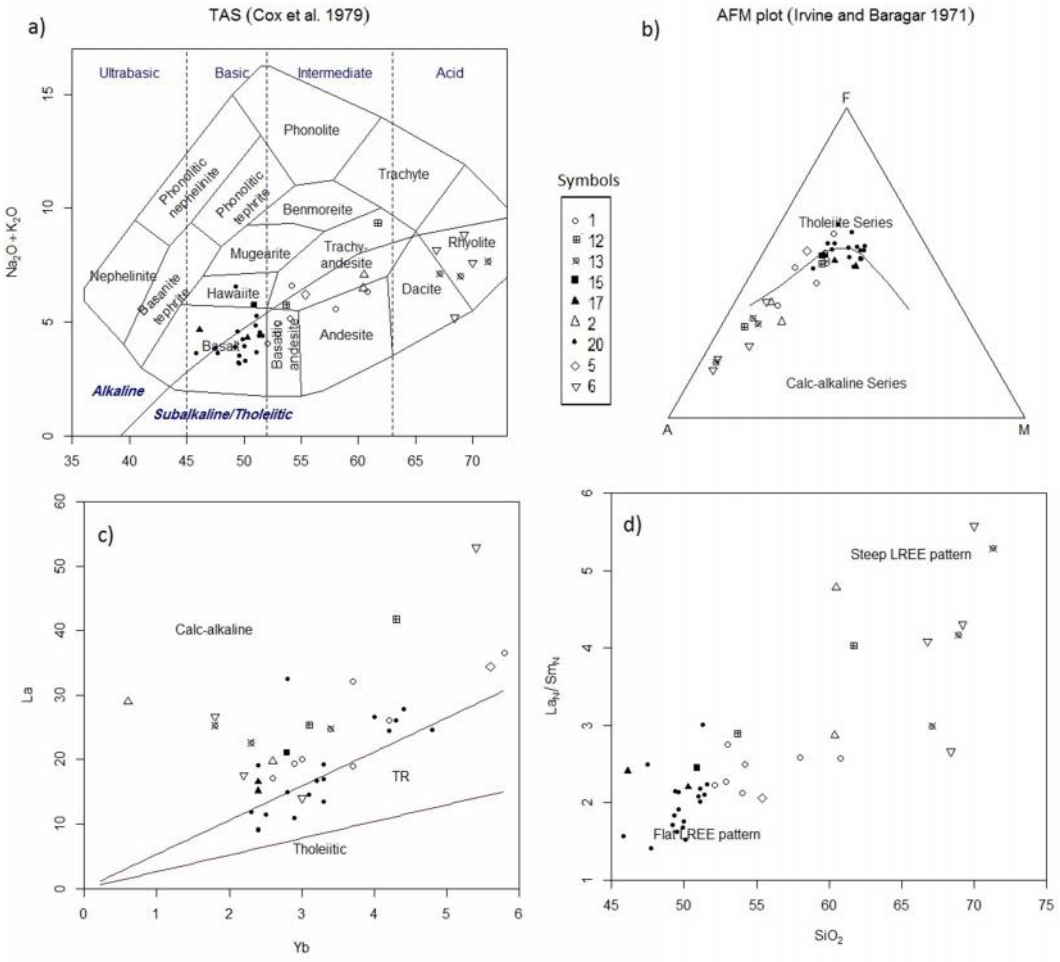

Figure 4. a) Total alkali versus silica plot showing the chemical classification of volcanic and subvolcanic rocks of HIC [38]; b) AFM plot [31]; c) La versus Yb plot; d) The plot of $(La/Sm)_{PM}$ vs. SiO_2, showing steepness or flatness of the LREE to MREE section of spider diagrams in rocks normalized with primitive mantle. Symbols: The symbols used in geochemical diagrams and plots: 1) Intemediate lava; 2) Intemediate subvolcanics; 5) Pyroclastics; 6) Acid subvolcanics; 12) Intemediate plutonics; 13) Acid lava; 15) Basic plutonics; 17) Basic subvolcanics; 20) Basic lava.

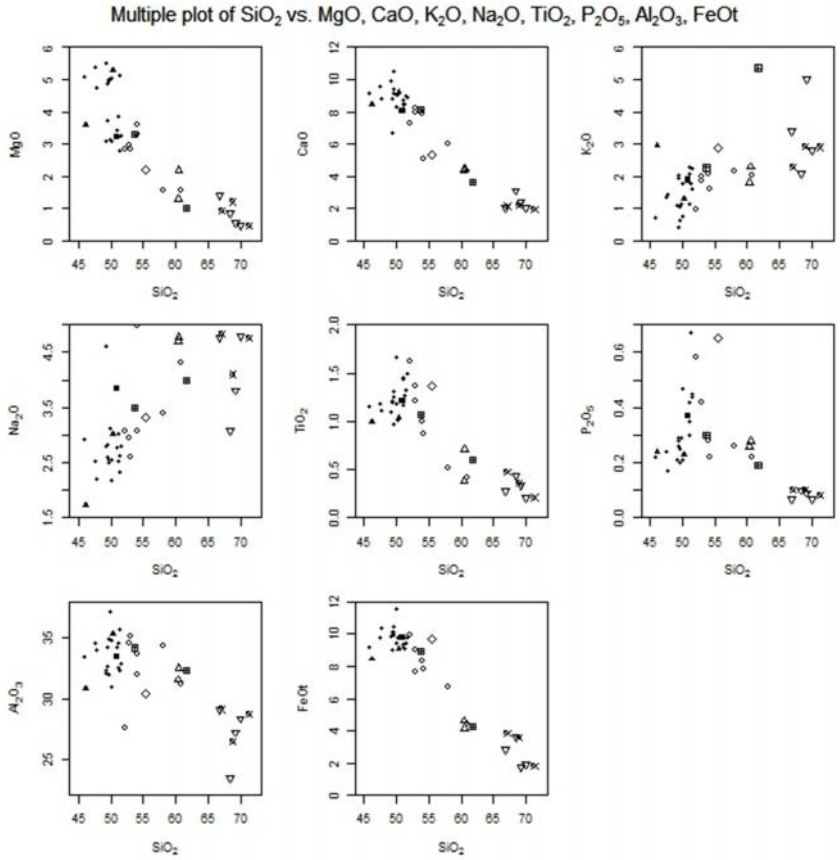

Figure 5. Harker diagrams for some oxides vs. SiO_2.

of Ni, Cr and MgO may indicate some aspects of magma evolution. It seems that samples 9 and 33 are the nearest samples to primitive magma, because of their highest contents.

Harker diagrams of some major oxides vs. SiO_2 or MgO (Figure 5) reveals the linear trends which indicates that differentiation may be the main process in formation of these rocks. The contents of FeOt, MgO, and CaO decreases with an increase in SiO_2 content. The trend which is consistent with differentiation of earlier phases as olivine, pyroxene and plagioclase and participation of oxide minerals (magnetite and/or ilmenite) in the fractionating assemblage. A clear bending in Harker diagrams of MgO, TiO_2, and Cr may be associated with differentiating minerals from olivine to pyroxene. Then, crystallization conditions have promoted the growth of plagioclase crystals after reaching the SiO_2 content of magma to 55%.

It has been found that REE (specially LREE) can be mobile during hydrothermal alteration and low-grade metamorphism [39]. To make sure of application of HFSE (esppecially REE) in interpretation of tectonic setting and petrogenesis of the studied rocks, the diagrams of LOI versus Nb/La or Th/La can be used [40]. Lack of correlation between LOI and these two ratios (diagrams not included) is a compelling evidence that the concentration of Th, Nb, and LREE have not been disturbed in HIC. Then these elements can be used for evaluation of petrogenesis and tectonic setting of igneous rocks. Although inverse relation between LOI and SiO_2 along with low-to-medium content of LOI and occurrence of quartz-calcite veins and epidote-chlorite in these rocks suggest low-grade metamorphism. In field and petrographic studies it has been seen that primary minerals partially or wholly altered to chlorite, epidote, and sericite; an observation which supports later hydrothermal alteration of these igneous rocks.

The ratio of $(La/Sm)_{PM}$ versus SiO_2 indicates that the pattern of normalized LREE to MREE is flatter in basic rocks and steeper in acid rocks because of enrichment of LREE in the latter.

Discussion

The extent of differentiation among different units

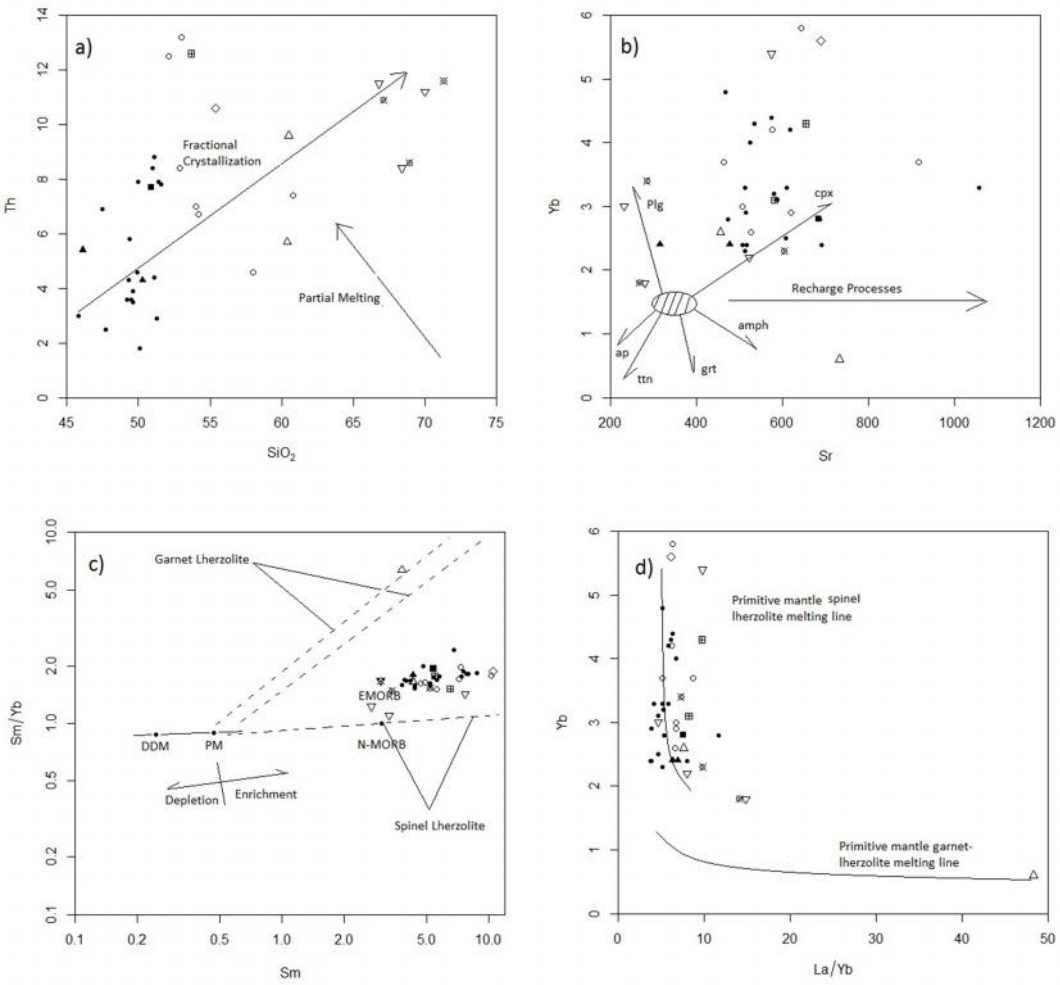

Figure 6. a) The trands of Fractional Crystallization and partial melting in the binary plot of Th vs. SiO_2; b) The diagram of Yb vs. Sr used for demonstration of fractional crystallization of some minerals [41]; c) REE model plot of Sm/Yb vs. Sm for HIC samples [42]. The heavy line represents the mantle array defined by DMM [45] and PM [46] compositions. The N-MORB and E-MORB compositions [46] have also been shown; d) REE model plot of Yb vs. La/Yb for HIC samples [47] from [14].

have been estimated from LREE/HREE ratio, which is demonstrated by La/Yb ratio (between 4 to 8 in most of our samples). Besides, the LILE/HFSE ratio can be shown in Sr/Y.

Differentiation trends of La-Yb (Figure 6b, c and d) has indicated the involvement of clinopyroxene and plagioclase minerals out of the stability domain of garnet, and apatite [27].

There are several REE model plots dealing with melting curves (lines) for spinel-lherzolite and garnet peridotite sources with depleted MORB mantle (DMM) and primitive mantle (PM) compositions. Different evidences support enriched spinel lherzolite as the magma source of the HIC. The garnet lherzolite is rejected except sample no. 1. All samples are probably co-magmatic and have origined from a single depth that have been lower than the depth of sample no. 1 (Figure 6c and d).

The effects of fractional crystallization and crustal contamination

Th-Yb-Nb systems are very useful in determining both the source diversity and crustal assimilation in basic rocks, because these elements as couples often are not dependent on fractional crystallization and/or partial melting [24], [26]. Th/Yb versus Nb/Yb and TiO_2/Yb versus Nb/Yb are two brand new diagrams that have been developed using the last version by [28]. Th/Yb versus Nb/Yb diagram (Figure 7) is developed for determining subduction-related settings and subduction-

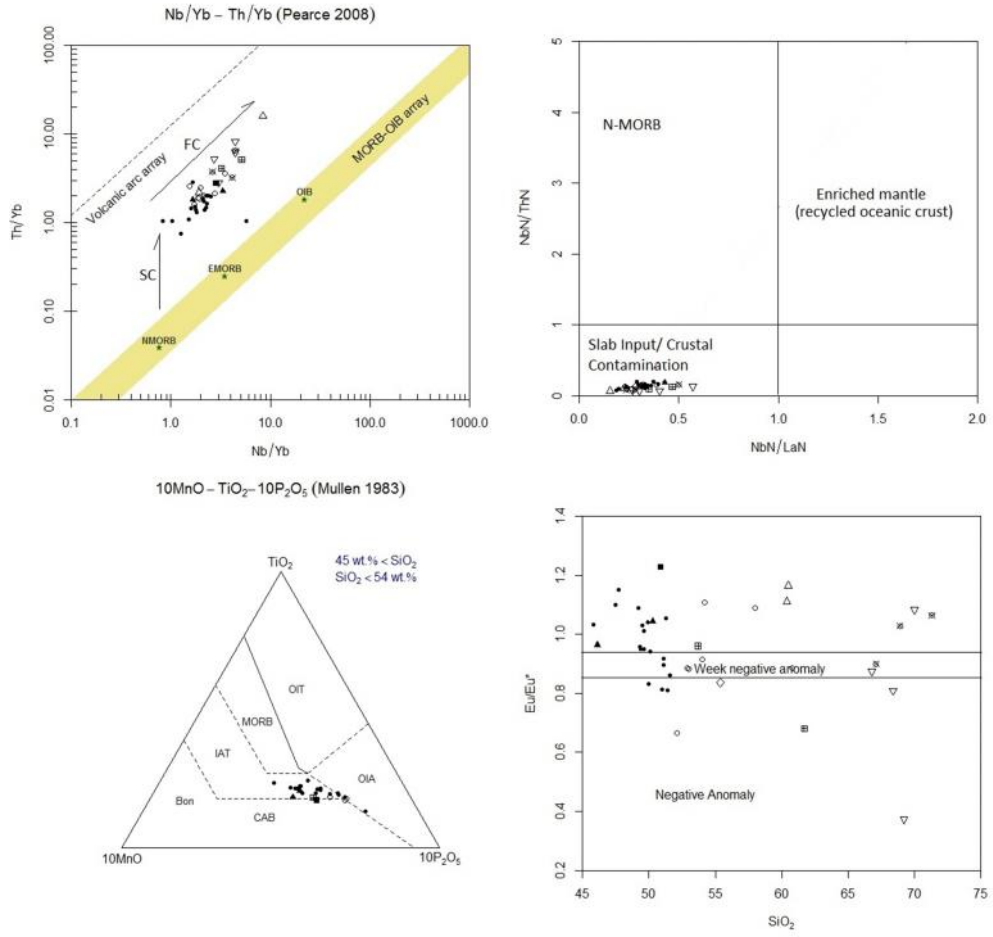

Figure 7. a) Th/Yb vs. Nb/Yb discriminating MORB-OIB array from volcanic arc array [28]; b) $(Nb/Th)_{PM}$ vs. $(Nb/La)_{PM}$ binary plot (after [48]). Numbers of two ratios are normalized with primitive mantle according to data from [49]); c) Ternary diagram of $MnO-TiO_2-P_2O_5$ [33]. Nearly all samples lie in the field of Island Arc Tholeiite (or Basalt); d) Negative Eu anomaly in some samples may indicate fractional crystallization of plagioclase in magma chamber.

unrelated ones [29], [30], though TiO_2/Yb versus Nb/Yb diagram (not shown) is used for systematics of the basaltic rocks independent to secondary alteration and enrichment processes related to subduction. Therefore it can be used for determining the compositions of the primitive mantle source of the volcanic rocks.

In the diagram of Th/Yb versus Nb/Yb (Figure 7) [28], volcanic rocks lie out of the mantle array (MORB-OIB array) which may suggest the effect of crustal contamination or the flow of fluids in the subduction zone. Such a contamination has increased the values of Th/Yb and has expelled the plot out of the mantle array. Evidently, our samples are higher than MORB-OIB array (or mantle array), suggesting that the source has subduction- related signatures. This is due to input of Th from subduction-related fluids or magma to their sources. The contamination of oceanic basalts with subducted sediments, oceanic crust and/or recycling crust, all can cause this displacement [31]. Besides, the magmatic evolution series parallel to MORB-OIB array can be due to the effects of fractional crystallization. It should be noted that, all samples have Nb/Yb ratios more than 1.0, suggesting an active continental margin as a source and rejecting an oceanic arc system.

In TiO_2/Yb versus Nb/Yb diagram, most of our basic samples concentrate around the transition line between E-MORB and N-MORB, although more evolved rocks show a trend to lower TiO_2/Yb values and higher Nb/Yb values, suggesting the effects of magmatic differentiation (probably due to elimination of TiO_2–bearing phases). This diagram can be used for determining the melting depth and then mantle temperature and thickness of the lithosphere during magma generation [31]. Lower TiO_2/Yb values in our samples (MORB-OIB array), indicate lower depth (and formation temperature) compared with OIB.

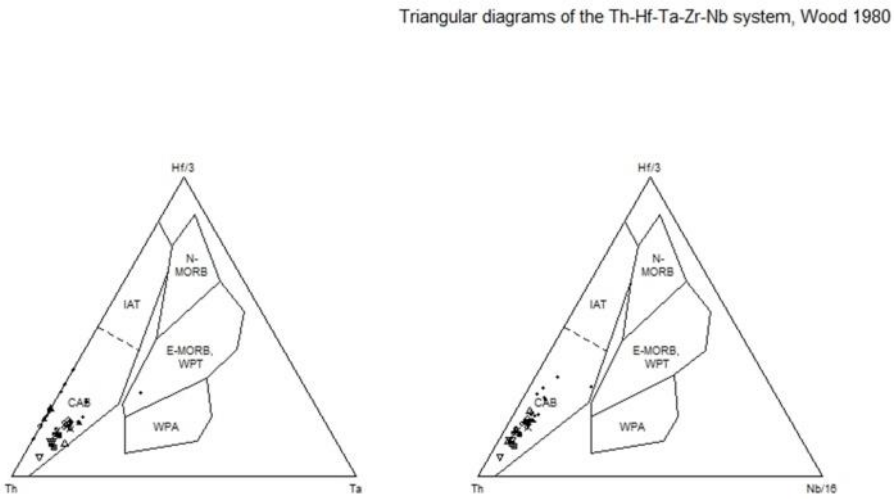

Figure 8. Ternary diagrams discriminating tectonic settings. The third triangular has been omitted due to lack of Zr data. The samples lie in the realm of calc-alkaline basalts.

All of the samples of HIC, fall in a field in $(Nb/Th)_{PM}$ vs. $(Nb/La)_{PM}$ diagram that suggest crustal contamination or input of the solutions from the subducted slab. Higher values of normalized Th and La content , shown by lower values of $(Nb/Th)_{PM}$ and $(Nb/La)_{PM}$ suggest higher degrees of crustal contamination. Magma and melting characteristics can be investigated through REE modeling.

Emplacement and tectonic setting

Immobile elements and their ratios can be used for determination of tectonic setting of the rocks studied. In order of achieving this goal, several discriminating diagrams should be used [26]. Many diagrams have been developed by different authors interpreting the tectonic setting of rock assemblages using major and trace elements. Major elements are still used in this kind of interpretations because of their simple application. But their mobility imposes some doubts to their usage in older altered or metamorphosed terrains [32]. Then, some diagrams are set aside in this study.

Using diagrams based on major elements such as [33], [34] is of concern in older terrains, because major elements may have different behavior during alteration or metamorphism. Then, it is recommended that the results shown by these diagrams rechecked using diagrams prepared with trace elements such as [35], [36] .

As it is evident in the following diagrams, all of the studied rock samples of HIC lie in the field of calc-alkaline and island arc basalts, i.e. destructive plate margin basalts and their differentiates. In triangular plots of [35], one sample lies outside of CAB field. It may occurred because Ta acts like Ti in differentiation of ferromagnesian and Fe minerals. Then, this sample may come close to the Ta apex, due to this differentiation. It should be noted that the border between IAT and CAB in D domain is not accepted by IUGS nomenclature recommendations, and these two domains are considered as a single domain, i.e. IAB.

The following multiple diagrams are more accurate because of multiple checking the geochemical conditions with tectonic settings. Evidently, log- ratios of major elements and trace elements [36] have shown the same results.

Spider diagram is another tool for interpreting magmatic evolution of igneous rocks and their emplacement and tectonic setting. The parallel patterns in all of the following diagrams may indicate comagmatic character of the studied rocks. Magma rising through a thick continental crust may be the source of crustal contamination, which has led to higher Rb/Sr and LILE/HFSE and has increased the Th content as a result of AFC processes [37].

The negative anomaly of Ti and Nb may indicate magmatic relation with subduction (e.g. calc-alkaline volcanic arc of continental active margin). This can be due to earlier depletion events in the mantle source. Two other minimum points – i.e. Ti and P- may be due to early crystallization of titano-magmetite and ilmenite and fractional crystallization of apatite, respectively. The concentration of incompatible elements – especially

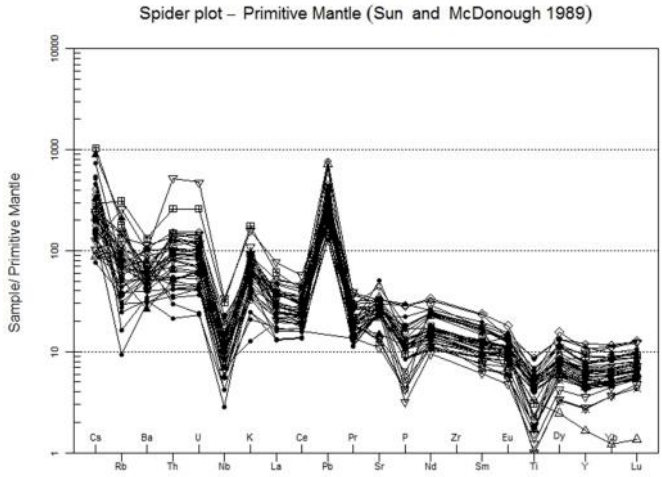

Figure 9. The spider plot of elemental values of HIC samples normalized with primitive mantle [46].

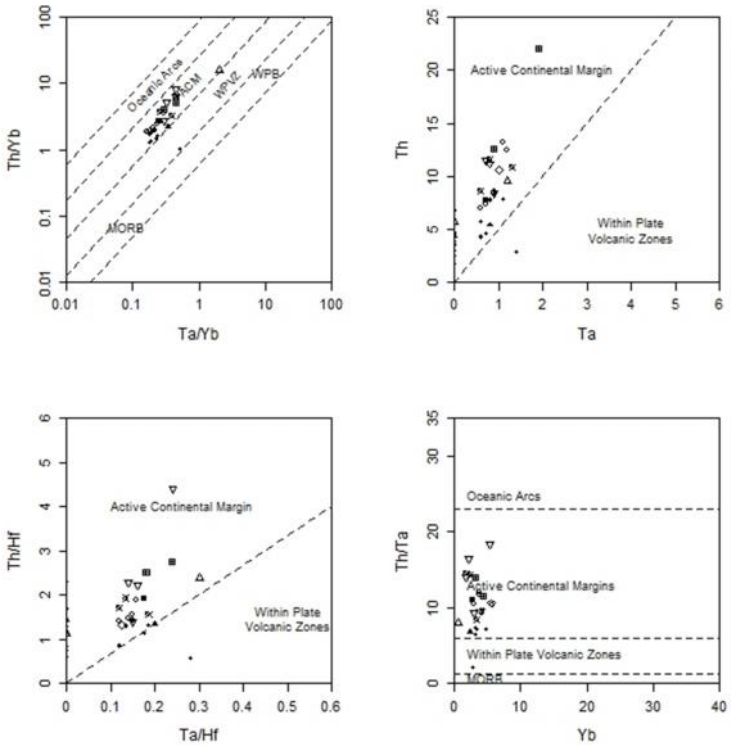

Figure 10. Geotectonic classification of volcanic rocks shows the affinity of ACM in HIC rocks [39].

REEs and LILEs- standardized with primitive mantle shows an enrichment of magma in Rb, Ba, K and Th. The above trends are evidences supporting that the HIC magma is contaminated with materials from deep continental crust. At the same time, magma was mixed with volatiles rich in early-melting components of oceanic crust. Lack of Sr and Eu anomaly in most of the rock samples may prove lack of fractional crystallization of plagioclase in magmatic melt. Enrichment of LREE –quantified as La/Sm ratio- and Eu anomaly, indicate higher degrees of REE differentiation. MREE to HREE are flat. Then there is no sign of garnet or spinel as the refractory phase during the melting. These conditions which are seen in few samples are due to eliminating plagioclase from the source or later, through fractional crystallization in

magma chamber before emplacement.

The troughs of Ti, Nb, and Ta are typical in calc-alkaline magma and may be interpreted with remained hornblende and Fe-Ti oxides in the source of parental magma. Both of Nb and Ta are very incompatible with typical mantle associations and are inactive during metasomatic events. Then their anomalies can be explained with adding slab elements from dehydrated oceanic crust into the mantle wedge, by which several incompatible elements – except Nb- are increased. All of samples show the same patterns in incompatible elements- i.e. they relatively have been enriched in highly-mobile elements (LILE) and have been depleted in immobile elements (HFSE).

Plutonic rocks' Trends

Plutonic rocks and acid rocks have not been encountered and studied in the previous works. As the plutonic rocks are very rare in HIC, only three samples are selected and studied geochemically (samples 18, 20, 22). In TAS diagram these three samples fall in gabbro-diorite domain [38]. In the following diagram, all of these plutonics and their volcanic equivalents lie in the field of ACM (i.e. active continental margin) [39]. This has been supported by other diagrams not included here (such as [40], [41] and by spider diagrams(Figure 9) (negative anomalies of Ti, Ta and Nb indicate the rocks of active continental margin related to subduction processes [42]. In the following diagrams plutonic rocks are demonstrated by squares, but other samples are plotted only for comparison.

Eruption in HIC include the phases of effusive and explosive activities. The eruption character has been variable from Strombolian to Vulcanian. In the plutonic dome of Kamali, near the summit dacite and trachite is formed. These more silicic lavas have indicate a more evolved melt. More differentiation has taken place near the surface and have led to an increase in SiO_2 content and a decrease in FeO content, which is evident in the previous Harker diagrams.

Conclusion

Hezar Igneous Complex (HIC) is originated by the intersection of north-south Sabzevaran fault and NW-SE Rafsanjan-Rayen fault. It is indicated that the possible place of the conduit and vent is in Jalas Mountain which has been splitted later by the first fault of the above faults into Minor and Major Jalas. The current summit, which was not the place of summit and vent in the time of its activity (because of abundant agglomerate spreading above it) had been arisen by ascending magma chamber under the HIC that constitutes the Kamali Mountain at the south of the summit. By the way, decisive verifying the place of main volcanic vent (or conduit) and the relation of main fault systems with HIC requires a thorough study of the structural features especially the faults and folds of the studied area and preparing a detailed structural map. Besides, isotopic and geochronological analyses can make more evidences for analyzing the extrusion of this complex and its relationship with other related structures such as Kamali Montain and Jalas Montain. The evidence of plutonic rocks of the Hezar intrusives are exposed in Kamali Mountain.

The subalkaline rocks of this complex are mainly composed of different pyroclastic and lava rocks, with an acidic to basic character showing the evidence of fractional crystallization and mineral segregation. The evidence of sequential explosive and effusive eruptions with Strombolian to Vulcanian types is evident. However, by structural evidences it is evident that the successions of events in HIC are as follow: 1): extrusion of pyroclastic and lava materials which are the main part of HIC; 2): Intrusion of Kamali, minor and major Jalases which were cut and splitted later by a N-S fault; 3): the last phase, intrusion of subvolcanic boddies in Jalas fractures. Besides there are some evidences of later alteration and metamorphism in northern and north-eastern flank which cause some valuable ancient structural and ornamental stone mines such as travertine and green marble. It seems that the later movement of the southern fault, i.e. Rafsanjan- Rayen fault, has devastated the southern part of the HIC including its main vent in Jalas and has made an appropriate place for ascending the lower plutonic rocks, exposed in Kamali Mountain. The most extensive extrusive materials include pyroclastic falls and flows such as volcanic tuffs, agglomerate, breccia and surge deposits. The less abundant successions of lava materials such as basalt and andesitic basalt are evident among these pyroclastic rocks.

Linear trend of Harker diagrams and its breaking indicates the fractional crystallization and the segregation of olivine and pyroxene, respectively. Low grade metamorphism along with the quartz, calcite, chlorite and epidote veins in these rock samples have some influences on relation of LOI and SiO2 without impacting Th, Nb, and LREEs.

The compositional trend of the rocks is more correlated with the melting of spinel lherzolite, not garnet lherzolite which can be attributed to a less formation depth of magma. Evolution of most of the samples have taken place out of the stability domain of garnet and apatite in a depth far less than the stability domain of garnet lherzolite.

The subduction-related mechanism of the magma

genesis has been indicated by IAB nature of the magma formation in geochemical diagrams. Certainly, the lack of Zr data in geochemical analyses of the studied samples imposed limitations in some geochemical diagrams and their resulted interpretations. All of the studied rock samples in HIC, fall in the realm of calc-alkaline basalts and island arc basalts, i.e. destructive plate margins.

Due to input of fluids from subducted slab or crustal contamination (higher content of Th and La), all of the studied rock samples lie out of the realm of MORB-OIB array (mantle array) and lie near the volcanic arc array. This factor suggests a source relating to subduction. Moreover, a magmatic evolution parallel with mantle array indicates fractional crystallization (FC), then this volcanic arc was an active continental margin, not an oceanic arc.

As it is evident in spider diagrams, all the samples are comagmatic. Due to higher content of Th and higher values of Rb/Sr and LILE/HFSE, ascending magma passed through a thicker continental crust. Negative anomaly in Ti, Nb and Ta suggests a magmatic relation with subduction (e.g. calk-alkaline volcanic arc in an active continental margin) in a calc-alkaline magma due to remaining Fe-Ti oxides in the source of parental magma. This may be the result of the earlier depletion events in a mantle source. Two other minimum points P and Ti can be due to early crystallization of titano-magnetite and ilmenite and fractional crystallization of apatite, respectively. The contamination of HIC magma with deep continental crust may be evident in an enrichment in Rb, Ba, K, and Th which are mixed with the constituent fluids of primary melting of oceanic crust. Lack of negative anomaly in Eu and Sr, suggests lack of fractional crystallization of plagioclase in magma.

The plutonic rocks (only two gabbro-diorite samples) lie in the realm of active continental margin (ACM) which is a kind of verification for the conclusion achieved by volcanic rocks.

Acknowledgement

This study was carried out through PhD thesis of the first author in Shahid Bahonar University of Kerman-Iran. Part of the costs of whole-rock geochemical analyses was provided through a research grant by IMIDRO (Iranian Mines & Mining Industries Development & Renovation). Whole-rock analyses were performed in SGS laboratories in Australia and Canada. Isotopic and dating analyses were carried out in Laboratory of Isotope Geology (Laboratório de Geologia Isotópica) of the University of Aveiro (Universidade de Aveiro), Portugal (LGI-UA). Abbas Hosseinipour, Ali Alirezaei, Masoud Moghaddas, Hassan Sadeghi, Ali Shahabi, Ali Naghdi, and Mahmoud Rahjou took part in field works. Some of tools and materials needed, prepared by Ahad Soltani from Keele University, UK, Saeid Aghaei and Dr. Ahmad Abbasnejad. Technical and Vocational University of Iran, specially Hatam Salimi (former president of Shahid Chamran Technical College) and Mohsen Lotfi (head of Neyshabur Technical College) are acknowledged for their official assistance with the first author. Finally, we want to thank warmly all guidance and points of view from Dr. Mohammad Hashem Emami, Dr. Mohsen Arvin, and Dr. Sara Dargahi.

References

1. Shafiei B. Lead isotope signatures of the igneous rocks and porphyry copper deposits from the Kerman Cenozoic magmatic arc (SE Iran) and their magmatic-metallogenetic implications. *Ore. Geol. Rev.* **38:** 27–36 (2010).
2. Chiu H. Y., Chung S. L., Zarrinkoub M. H., Mohammadi S. S., Khatib M. M., and Iizuka Y. Zircon U–Pb age constraints from Iran on the magmatic evolution related to Neotethyan subduction and Zagros orogeny. *Lithos.* **162–163:** 70–87 (2013).
3. Kananian A., Sarjoughian F., Nadimi A., Ahmadian J. and Ling W. Geochemical characteristics of the Kuh-e Dom intrusion, Urumieh–Dokhtar Magmatic Arc (Iran): Implications for source regions and magmatic evolution. *J. Asian Earth Sci.* **90:** 137–148 (2014).
4. Mirzaie A., Bafti S. S. and Derakhshani R. Fault control on Cu mineralization in the Kerman porphyry copper belt, SE Iran: A fractal analysis. *Ore Geol. Rev.* **71:** 237–247 (2015).
5. Alimohammadi M., Alirezaei S. and Kontak D. J. Application of ASTER data for exploration of porphyry copper deposits: A case study of Daraloo–Sarmeshk area ، southern part of the Kerman copper belt ،Iran. *Ore Geol. Rev.* **70:** 290–304 (2015).
6. Omrani J, Agard P, Whitechurch H, Benoit M, Prouteau G and Jolivet L. Arc-magmatism and subduction history beneath the Zagros Mountains ،Iran: A new report of adakites and geodynamic consequences. *Lithos.* **106:** 380–398 (2008).
7. Richards J. P. Tectonic, magmatic and metallogenic evolution of the Tethyan orogen: From subduction to collision. *Ore Geol. Rev.* **70:** 323–345 (2015).
8. Zarasvandi A., Rezaei M., Raith J., Lentz D., Azimzadeh A.M. and Pourkaseb H. Geochemistry and fluid characteristics of the Dalli porphyry Cu–Au deposit ، Central Iran. *J. Asian Earth Sci.* **111:** 175–191 (2015).
9. Zarasvandi A., Rezaei M., Sadeghi M., Lentz D., Adelpour M. and Pourkaseb H. Rare earth element signatures of economic and sub-economic porphyry copper systems in Urumieh–Dokhtar Magmatic Arc (UDMA) Iran. *Ore Geol. Rev.* **70:**407–423 (2015).

10. Agard P., Omrani J., Jolivet L. & Mouthereau F. Convergence history across Zagros (Iran): constraints from collisional and earlier deformation. *Int. J. Earth Sci.* **94:** 401–419 (2005).
11. Chiu H. Y., Chung S. L., Zarrinkoub M. H., Mohammadi S. S., Khatib M. M., and Iizuka Y. Zircon U–Pb age constraints from Iran on the magmatic evolution related to Neotethyan subduction and Zagros orogeny. *Lithos* **162-163:** 70–87 (2013).
12. Hosseini M. R., Hassanzadeh J., Alirezaei S., Sun W. & Li C.Y. Age revision of the Neotethyan arc migration into the southeast Urumieh-Dokhtar belt of Iran: Geochemistry and U–Pb zircon geochronology. *Lithos* **284–285:** 296–309 (2017).
13. Hosseini M. R., Ghaderi M., Alirezaei S. & Sun, W. Geological characteristics and geochronology of the Takht-e-Gonbad copper deposit ،SE Iran: A variant of porphyry type deposits. *Ore Geol. Rev.* **86:** 440–458 (2017).
14. Niktabar S. M., Moradian A., Ahmadipour H., Santos J. F. and Mendes M. H. Petrogenesis of Lalehzar granitoid intrusions (Kerman Province- Iran). *J. Sci.* **26 (4)**: 333-348 (2016).
15. Khajehjavaran Z. Petrology, geochemistry and petrogenesis in the western part of Hezar complex (Southwest of Rayen Kerman province). MSc. Thesis (Shahid Bahonar University of Kerman, 2010).
16. Maleki L. Petrology and volcanology of Hezar complex (southwest of Rayen- Kerman province). MSc. Thesis (Shahid Bahonar University of Kerman, 2004).
17. Dimitrijevic M. D. *Geology of Kerman Region*. (Geological Survey of Iran, 1973).
18. Noorizadeh M., Moradian A., Ahmadipour H. and Ghassemi M. R. Analysis of Geotourism Strategies in Rayen- Kerman Using SWOT method. in *The 2nd National Conference on Iranian Tourism and Ecotourism* (2013).
19. Noorizadeh M., Moradian A., Ahamadipour H. and Ghassemi M. R. Description and Classification of Geotourism Capabilities of the Ancient City- Rayen-Kerman Province. in *The 1st Conference on Tourism, National Wealth and Future Perspectices* (2015).
20. Sa,adat A., Soltanpour A. and Seddighi M. Measurement of the minimum gravity of Iran. in *Geomatics* **88:** 11 (2009).
21. Noorizadeh M., Moradian A., Ahmadipour H. and Ghassemi M. R. Structural and Petrographic Evidence of Alteration around the Hezar Volcanic Complex (South of Kerman- Iran). in *The 1st International Congress on Earth Sciences* (2014).
22. Winter J. Introduction to Igneous and Metamorphic Petrology Prentice-Hall Inc. *Up. Saddle River N. J.* **7458** (2001).
23. Winchester J. and Floyd P. Geochemical discrimination of different magma series and their differentiation products using immobile elements. *Chem. Geol.* **20:** 325–343 (1977).
24. Pearce J. A. Role of the sub-continental lithosphere in magma genesis at active continental margins. 230-249 (1983).
25. Whitford D., Korsch M., Porritt P. and Craven S. Rare-earth element mobility around the volcanogenic polymentallic massive sulfide deposit at Que River, Tasmania, Australia. *Chem. Geol.* **68:** 105–119 (1988).
26. Nude P.M., Kwayisi D., Taki N.A., Kutu J.M., Anani C.Y., Banoeng-Yakubo B., Asiedu D.K. Petrography and chemical evidence for multi-stage emplacement of western Buem volcanic rocks in the Dahomeyide orogenic belt ، southeastern Ghana, West Africa. *J. Afr. Earth Sci.* **112, Part A:** 314–327 (2015).
27. Béguelin P., Chiaradia M., Beate B. and Spikings R. The Yanaurcu volcano (Western Cordillera ،Ecuador): A field, petrographic, geochemical, isotopic and geochronological study. *Lithos* **218:** 37–53 (2015).
28. Pearce J. A. Geochemical fingerprinting of oceanic basalts with applications to ophiolite classification and the search for Archean oceanic crust. *Lithos* **100:** 14–48 (2008).
29. Dilek Y. and Furnes H. Ophiolite genesis and global tectonics: geochemical and tectonic fingerprinting of ancient oceanic lithosphere. *Geol. Soc. Am. Bull.* **123:** 387–411 (2011).
30. Dilek Y. and Furnes H. Ophiolites and their origins. *Elements* **10:** 93–100 (2014).
31. Pease V., Scarrow J., Silva I. N. and Cambeses A. Devonian magmatism in the Timan Range ،Arctic Russia—subduction ،post-orogenic extension ،or rifting? *Tectonophysics* **691**: 185-197 (2016).
32. Verma S. P. Statistical evaluation of bivariate ،ternary and discriminant function tectonomagmatic discrimination diagrams. *Turk. J. Earth Sci.* **19:** 185–238 (2010).
33. Mullen E. D. $MnO/TiO_2/P_2O_5$: a minor element discriminant for basaltic rocks of oceanic environments and its implications for petrogenesis. *Earth Planet. Sci. Lett.* **62:** 53–62 (1983).
34. Verma S. P., Guevara M. and Agrawal S. Discriminating four tectonic settings: Five new geochemical diagrams for basic and ultrabasic volcanic rocks based on log—ratio transformation of major-element data. *J. Earth Syst. Sci.* **115:** 485–528 (2006).
35. Wood D. A. The application of a Th Hf Ta diagram to problems of tectonomagmatic classification and to establishing the nature of crustal contamination of basaltic lavas of the British Tertiary Volcanic Province. *Earth Planet. Sci. Lett.* **50:**11–30 (1980).
36. Agrawal S., Guevara M. and Verma S. P. Tectonic discrimination of basic and ultrabasic volcanic rocks through log-transformed ratios of immobile trace elements. *Int. Geol. Rev.* **50:** 1057–1079 (2008).
37. Tamura Y., Ishizuka O., Stern R.J., Shukuno H., Kawabata H., Embley R.W., Hirahara Y., Chang Q., Kimura J.I., Tatsumi Y., Nunokawa A. Two primary basalt magma types from northwest Rota-1 volcano ،Mariana arc and its mantle diapir or mantle wedge plume. *J. Petrol.* **52(6)**:1143-83 (2011).
38. Cox K. J., Bell J. D. and Pankhurst R. J. *The Interpretation of Igneous Rocks*. (Allen and Unwin ،1979).
39. Schandl E. S. and Gorton M. P. Application of high field strength elements to discriminate tectonic settings in VMS environments. *Econ. Geol.* **97:** 629–642 (2002).
40. Harris N. B., Pearce J. A. and Tindle A. G. Geochemical characteristics of collision-zone magmatism. *Geol. Soc. Lond. Spec. Publ.* **19:** 67–81 (1986).
41. Pearce J. A., Harris N. B. and Tindle A. G. Trace element discrimination diagrams for the tectonic interpretation of

granitic rocks. *J. Petrol*. **25**: 956–983 (1984).
42. Gil-Rodriguez J. Petrology of the Betulia Igneous Complex, Cauca, Colombia. *J. South Am. Earth Sci.* **56:** 339–356 (2014).
43. Irvine T. and Baragar W. A guide to the chemical classification of the common volcanic rocks. *Can. J. Earth Sci.* **8** 523–548 (1971).
44. Aldanmaz E., Pearce J. A., Thirlwall M. and Mitchell J. Petrogenetic evolution of late Cenozoic ،post-collision volcanism in western Anatolia, Turkey. *J. Volcanol. Geotherm. Res.* **102:** 67–95 (2000).
45. McKenzie D. and O'nions R. Partial melt distributions from inversion of rare earth element concentrations. *J. Petrol.* **32:** 1021–1091 (1991).
46. Sun S. S. and McDonough W. Chemical and isotopic systematics of oceanic basalts: implications for mantle composition and processes. *Geol. Soc. Lond. Spec. Publ.* **42:** 313–345 (1989).
47. Peters T. J., Menzies M., Thirlwall M. and Kyle P. R. Zuni–Bandera volcanism, Rio Grande, USA—Melt formation in garnet-and spinel-facies mantle straddling the asthenosphere–lithosphere boundary. *Lithos* **102:** 295–315 (2008).
48. Piercey S.J., Nelson J.L., Colpron M., Dusel-Bacon C., Simard R.L., Roots C.F. Paleozoic magmatism and crustal recycling along the ancient Pacific margin of North America ،northern Cordillera. *Paleoz. Evol. Metallog. Pericratonic Terranes Anc. Pac. Margin N. Am. Can. Alaskan Cordill. Geol. Assoc. Can. Spec. Pap.* **45:** 281–322 (2006).
49. McDonough W. F. and Sun S.-S. The composition of the Earth. *Chem. Geol.* **120:** 223–253 (1995).
50. Nakamura N. Determination of REE, Ba, Fe, Mg, Na and K in carbonaceous and ordinary chondrites. *Geochim. Cosmochim. Acta*. **38:** 757–775 (1974).